



## Functional Surface of the golden mussel's foot: morphology, structures and the role of cilia on underwater adhesion



Gabriela Rabelo Andrade <sup>a,\*</sup>, João Locke Ferreira de Araújo <sup>a,1</sup>, Arnaldo Nakamura Filho <sup>a</sup>, Anna Carolina Paganini Guañabens <sup>a</sup>, Marcela David de Carvalho <sup>b</sup>, Antônio Valadão Cardoso <sup>c,d,e</sup>

<sup>a</sup> Bioengineering Centre of Invasive Species – CBEIH, Av. José Cândido da Silveira, 2000, Horto, Belo Horizonte, Minas Gerais 31035-536, Brazil

<sup>b</sup> Companhia Energética de Minas Gerais – CEMIG, Av. Barbacena, 1200, Santo Agostinho, Belo Horizonte, Minas Gerais 30190-131, Brazil

<sup>c</sup> University of the State of Minas Gerais – UEMG, Av. Antônio Carlos, 7545, São Luiz, Belo Horizonte, MG CEP 31270-010, Brazil

<sup>d</sup> CBEIH-CITSE Center of Innovation and Technology SENAI-FIEMG - campus CETEC, Brazil

<sup>e</sup> Av. José Cândido da Silveira, 2000 - Horto - Belo Horizonte - Minas Gerais, 31035-536 - Brazil

### ARTICLE INFO

#### Article history:

Received 10 July 2014

Received in revised form 14 January 2015

Accepted 21 April 2015

Available online 23 April 2015

#### Keywords:

Biological material

Functional surface

Morphology

Cilia

Van der Waals forces

Mussel

### ABSTRACT

In this study we characterized the surface morphology and ultrastructure of the foot of the golden mussel, *Limnoperna fortunei* (Dunker, 1857), relating its characteristics to the attaching mechanisms of this mollusk. The observation of the foot of this bivalve reveals the presence of micro-scaled cilia with a unique shape, which has a narrowing at its end. This characteristic was associated to the capacity for underwater adhesion to substrates through the employment of van der Waals forces, resembling the adhesion phenomenon of the gecko foot. The temporary attachment during locomotion by means of the foot to substrates was observed to be strong even on smooth surfaces, like glass, or hydrophobic waxy surfaces. Comparing TEM and light microscopy results it was possible to associate the mucous secretions and secreting cells found along the tissues to the production of the byssus inside the groove on the ventral portion of the foot. Not only our experiments, but also the state of the art allowed us to discard the involvement of secretions produced in the foot of the mussel to the temporary adhesion. Through SEM images it was possible to build a virtual three-dimensional model where total foot surface was measured for the estimated calculation of van der Waals forces. Also, some theoretical analysis and considerations have been made concerning the characteristics of the functional surface of *L. fortunei* foot.

© 2015 Elsevier B.V. All rights reserved.

### 1. Introduction

The morphology and behavior of living beings cannot be analyzed separately from their structure and materials. Biological material properties emerge from its complex hierarchical structures formed by a variety of natural polymers and basic minerals and exhibit exceptional physical properties such as high hardness, flexibility, pressure resistance and compression, among others. The biological surfaces are an even more peculiar case and constitute the interface between living beings and the environment and serving to different purposes on each species [1]. Among some properties, we can highlight the physical, chemical and thermal protection; sensory activity; secretion and transport of substances; anti-wetting; and adhesion reduction or enhancement. The study of adhesive properties of biological surfaces has earned prominence specially after the publication of investigations

about gekkonid feet adhesion and the later development of bioinspired dry adhesives [2,3].

The bonding attachment mechanisms found in animals were classified by Barnes [4] into three main types: suction, wet adhesion and the last one that is of our interest: dry adhesion using intermolecular interactions such as van der Waals forces.

Adhesive apparatus are also found in several species of mollusks and serve to locomotory, and temporary and permanent attachments to substrates. Primitive mollusks had flattened and ciliated foot well supplied with mucous gland cells and the foot was kept by the bivalves throughout evolution, having left its flat creeping sole shape, as can still be observed in gastropods, to become blade-like as these animals became laterally compressed [5]. Especially in the case of epifaunal bivalves such as mussels, it is known that the foot also retained their motor skills used primarily in the juvenile stage, emerging from the larval stage, but that can also be observed in use during adulthood.

The foot of attaching bivalves (mussels) is closely linked to the production of byssus, an essential apparatus for the maintenance of the epifaunal lifestyle. Byssi are extracellular proteinaceous complex that helps mussels in permanent underwater adhesion. They are composed by a root, which is located inside foot's tissue, a stem and threads that

\* Corresponding author.

E-mail addresses: [gabrielarabelo@gmail.com](mailto:gabrielarabelo@gmail.com) (G.R. Andrade), [joalocke.bio@gmail.com](mailto:joalocke.bio@gmail.com) (J.L.F. Araújo).

<sup>1</sup> These authors contributed equally to the present study.

emerge from it and adhesive plaques at each thread extremity [6,7]. Besides its contribution to the permanent adhesion to substrates through the formation of highly adhesive proteins for the production of the byssus [8–11], the foot of the mussels possesses marked importance in the process of active locomotion and temporary attachment, being present from the larval phase as their first structure of adherence to substrates. As it can be seen on studies of mollusks such as the gastropod *Haliotis rufescens* [12] and in attaching bivalves such as the mussels *Mytilus edulis* [13], *Perna viridis* [14], *Septifer virgatus* [15] and *Tegillarca granosa* [8].

The freshwater bivalve *Limnoperna fortunei* known as the golden mussel belongs to the family Mytilidae of marine mussels, order Mytiloida and subclass Pteriomorpha. Their original geographical distribution was restricted to Southeast Asia and it has been found as an invasive species for the first time in 1966, in Hong Kong, and in 1991 in Japan and South America. The economical impacts caused by the species are notable since it frequently blocks water impoundment pipelines, grids and cooling systems of hydropower plants and network tanks in fish farms. These factors arise out of the high adhesive capacity of the species intensified by its gregarious behavior [16,17].

Considering the relevance of the foot of the mussel *L. fortunei* to the permanent attachment processes and also its remarkable capacity of temporary underwater adhesion through the role of its ciliated surface, this study aimed at understanding the structure of this organ. In order to characterize the morphology and adhesion apparatus of the functional surface of the foot, microscopy techniques, image post-processing and theoretical measurements were used. For image generation the techniques of scanning electron microscopy and transmission electron microscopy have been used also as light microscopy. The images produced have been processed for generating a 3D virtual object from what volume and surface area have been taken. The measurements obtained have been used for further estimation of van der Waals forces.

## 2. Materials and methods

### 2.1. Specimens

The specimens of *L. fortunei* were collected in the River Paranaíba, downstream of the confluence with the Barreiro river (navigation buoy 30 – Paranaíba river basin – latitude: 19.655834° S/longitude: 51.083889° W) near the Municipality of Parnaíba (MS). The animals were removed from navigation buoys with the help of spatulas. Subsequently they were transported to the laboratory, where they were dissected and the feet were kept at the refrigerator temperature (10 °C) for 24 h until the experiment is performed.

The specimens were prepared for foot examination under scanning electron microscopy (0.5 cm<sup>3</sup>) and transmission electron microscopy (2 mm<sup>3</sup>) following specific protocols for each process (Section 2.2).

In order to provide additional information about the secretions and its correlation to the foot groove the specimens were subsequently stained with Hematoxylin–Eosin (H–E) and examined under light microscopy (Section 2.3).

10 young animals between 6.2 mm and 7.2 mm have been collected for weighing measurement. Weight was taken using a Tepron accurate balance of 3 decimal places. The measurements resulted in a mean weight of 0.08796 g per individual. Also 20 adult animals between 2.4 cm and 3.4 cm have been collected for weighing, volume and density measurement. Weight was taken using a Tepron accurate balance of 3 decimal places. With the help of two beakers of 20 ml and 5 ml the displaced liquid volume of each mussel has been collected and later measured. The measurements were taken to further calculate the average density.

### 2.2. Electron microscopy

The specimens were fixed in modified Karnovsky solution (2.5% glutaraldehyde and 2% paraformaldehyde) and 0.1 M phosphate buffer,

pH 7.3 during 48 h at 4 °C. The dehydration was performed by passing the specimen three times for 10 min through each dilution of an alcoholic series (70–100%) and the samples were post-fixed in 1% Osmium Tetroxide (OsO<sub>4</sub>) for 2 h at room temperature. Experiments and analyses involving electron microscopy were performed in the Centre of Microscopy at the Universidade Federal de Minas Gerais, Belo Horizonte, MG, Brazil.

#### 2.2.1. Scanning electron microscopy (SEM)

The samples were submitted to a Bal-Tec Critical Point Dryer, RES101 Model (Leica). The surface was coated with gold ion particles (10 nm thickness) in a Bal-Tec metalizer, Model MD20 (Leica). The visualization of the samples occurred in two models of scanning electron microscope: FEG – Quanta 200 FEI and JEOL JSM – 6360LV.

In order to obtain images in transverse and longitudinal sections, some samples were submitted to cryofracture technique. The procedure followed the same method of the previous samples, but before submitting the specimens to the critical point drying with CO<sub>2</sub>, the cells were frozen to the temperature of liquid nitrogen (–196 °C) and fractured with a scalpel blade.

#### 2.2.2. Transmission electron microscopy (TEM)

The samples were submitted to a Bal-Tec Critical Point Dryer, RES101 Model (Leica). After dehydration, the samples were embedded in Epon plastic resin. The ultrathin sections were contrasted with uranyl acetate and lead citrate and were examined utilizing the Transmission Electron Microscope Tecnai G2-20 – SuperTwin FEI – 200 kV.

### 2.3. Light microscopy

The specimens were fixed in Bouin's fluid during 24 h. At the end of fixation, the specimens were rinsed several times in running water for 60 min until no more yellowish color could be seen. They were then transferred to 70% ethanol and dehydration was performed by passing the specimen three times for 10 min through each dilution of an alcoholic series (70–100%).

The slides were diaphanized in xylene for three sequenced times of 5 min each. The specimens were then embedded in paraffin and subsequently sectioned at 4–6 μm thickness using a microtome (RM2235, Leica, Germany). Specimens were stained with Hematoxylin–Eosin (H–E).

### 2.4. Analyses of the images

SEM images were analyzed in the software *ImageJ* (public domain software developed in the National Institutes of Health, USA) for measurements of the average length and diameter of the cilia stem and average length and diameter of the distal portion of the cilia. To verify the average results, various measurements were made on similar structures from different images (22 diameters; 12 total lengths; 13 diameters and 13 lengths of the distal portion) and the arithmetic mean was calculated from them (Fig. 1). Also based on cryofracture SEM images the average density of cilia was calculated resulting on an average of 28.5 cilium per square micrometer.

### 2.5. 3D model analyses

In order to estimate the adhesion by Van der Waals forces of an individual, a three-dimensional model was obtained from computational processing of SEM images. The model was subsequently measured using specific software. The individual used to obtain the images was a young adult mussel with 6.4 mm shell length.

#### 2.5.1. Photogrammetric 3D processing

SEM images have been produced with regular variations of angle (in the axes x and y) covering the entire sample and extra images have also

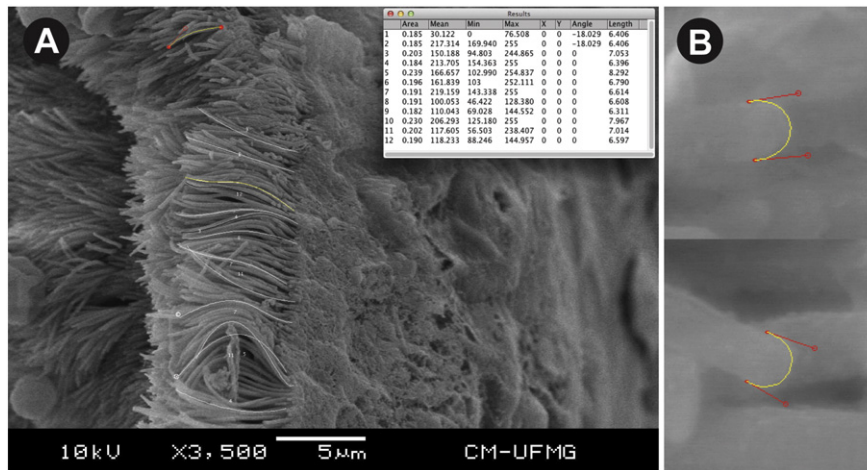


**Fig. 1.** Measurements of the cilia of the foot of the mussel *L. fortunei* measured on ImageJ. (A) Average length of the cilia measurements. This present image was obtained using cryo-fracture technique which made possible to observe the hole extension of each cilium. The table in the upright corner is a compilation of the measures generated on ImageJ. (B) Measurements of the rounded tip of the cilia through the construction of Bezier curves.

been produced to show complex surfaces or negative angles in a total of 64. On the software Agisoft Photoscan Pro (version 1.0.3) the images have been aligned (Fig. 2A), processed for the formation of a dense cloud of points (Fig. 2B) and later processed into a three-dimensional surface mesh (Fig. 2C).

### 2.5.2. 3D measurements

The 3D virtual model was then processed in Autodesk Meshmixer (version 5.10.79), in which the foot has been isolated from the rest of the model (Fig. 3A) and the open boundaries have been fixed. The final model (Fig. 3B) was used to obtain an estimated value of volume and total surface area. The estimated values were then used for quantitative calculation of the adhesion and pull-off forces.

## 3. Results

### 3.1. General morphology and structures of the foot observed by light and electronic microscopy

The foot of the *L. fortunei* was characterized as flattened and fused with the visceral mass (Fig. 4). The epithelial layer is formed by simple columnar epithelium containing or not mucous cells. The form of the

epithelium is different depending on the region where it is found; being composed of ciliated columnar tissue along the whole extension of the foot and simple columnar in the portions nearer the visceral mass of the animal.

The foot of the *L. fortunei* is composed of epithelial, connective and muscular tissue layers, presenting a groove in the ventral portion, which measures around 60% of the length of the foot, with a duct in its base, from where the byssus threads issue (Figs. 4 and 5).

#### 3.1.1. Groove and glandular secretions

Through the SEM images it was possible to observe a depression in the ventral part of the foot (Fig. 5F), denominated in the literature as “groove”. This structure is related to the mussel attachment process to the substrate, being involved in the production of secretions that will give form to the byssus and was already observed in another species of attaching mussel, *M. edulis* [13,18].

Some images produced of the ventral region of the foot showed the existence of cilia also covering the inside of this channel with secretions deposited on the surface of these cilia (Fig. 6).

The groove is delimited by ciliated epithelial tissue that can be seen in the ventral region of the foot within which glandular secretions could

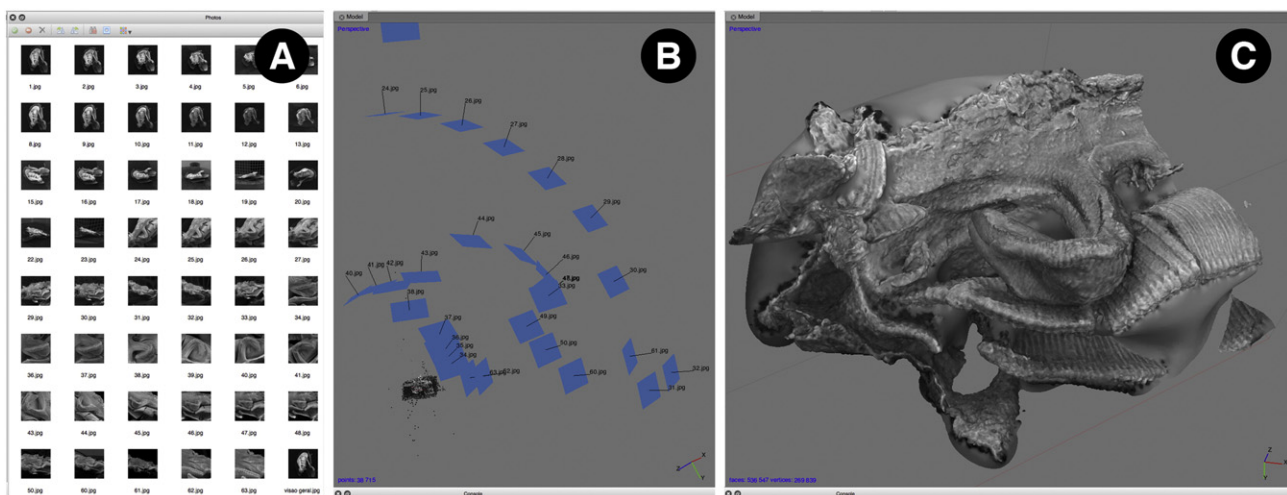


**Fig. 2.** Three steps of photogrammetric processing of SEM images on Agisoft Photoscan Pro. (A) Mosaic of images used for the composition of dense cloud of points. (B) Image alignment and dense cloud of points. (C) 3D mesh built from the processing of dense cloud of points into mesh. It is possible to observe the three-dimensional structure of the foot and also some gills below it.

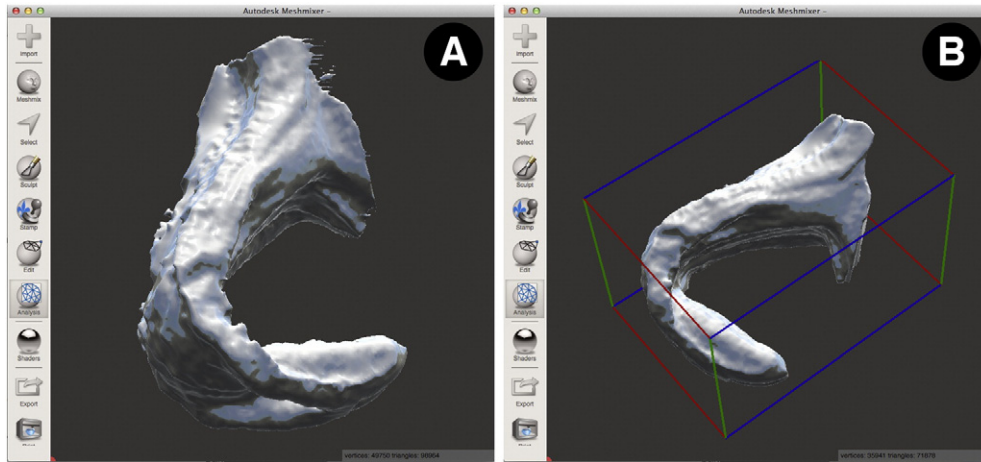


**Fig. 3.** 3D processing of the 3D model generated from SEM images. (A) Beginning of the processing of the 3D model of the foot where open boundaries and remaining untied parts can be seen. (B) Final model of the foot from which measurements of volume and surface area were extracted.

be found both by electron microscopy (Fig. 6D) and light microscopy (Fig. 7).

Transmission electron microscopy (TEM) revealed the presence of at least three types of secretory cells related to the area of the groove. The secreting cells found could be distinguished in accordance with the cellular form and density of the secretion beads and were classified into three types (A, B and C).

*Type A:* the most common type among the three types of secretory cells and more present in the epithelial layer. The secretion granules

have lower density among the three types of secretory cells, indicated by lighter shades of gray (Fig. 8A).

*Type B:* the cells of this tissue are oval-shaped and were mainly observed in the connective tissue layer. The secretory granule has a rounded shape with a mean diameter of  $0.8 \mu\text{m}$ . Electron density in the membrane was higher than in A, but was lower than in C (Fig. 8B). These structures also have a peculiar pattern inside, in which the secretion product resembles to be granular as well.

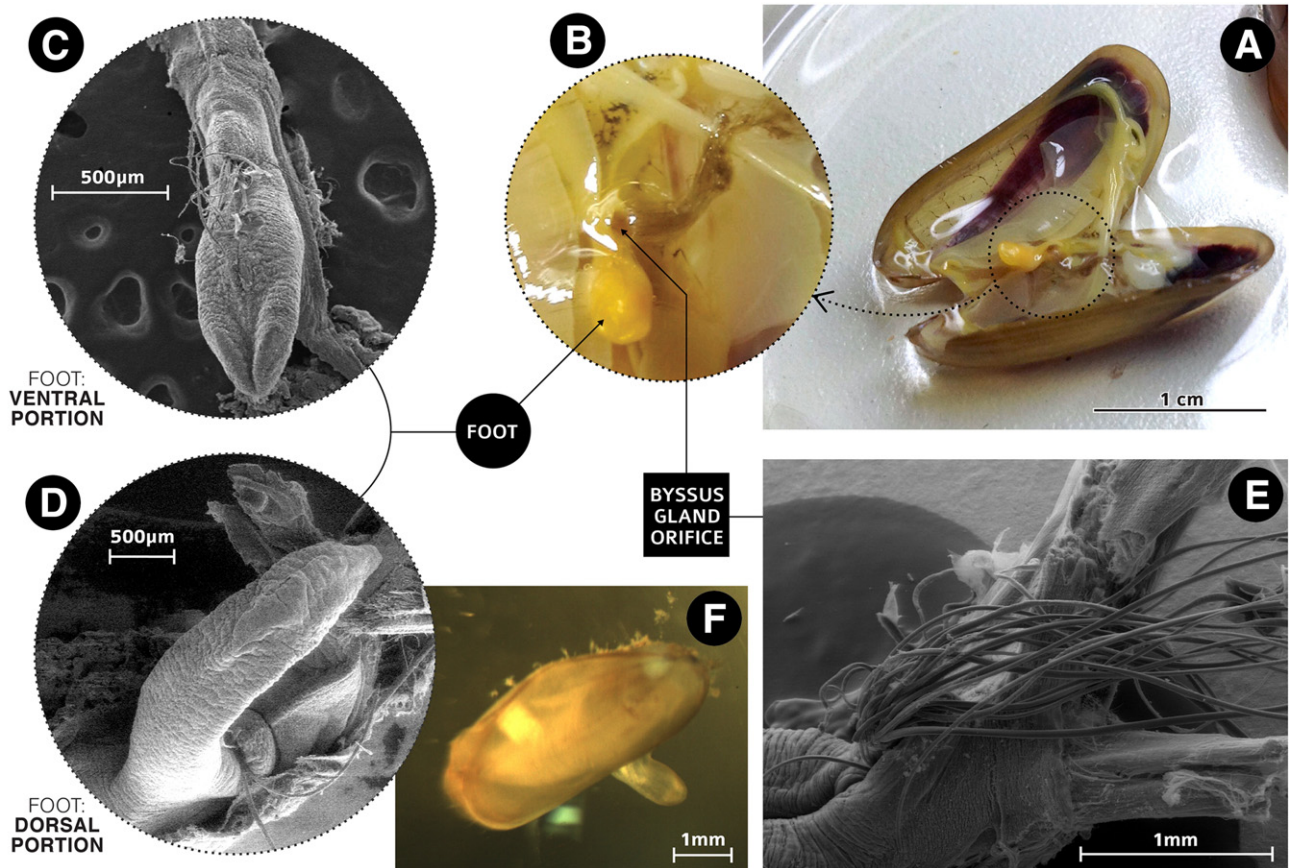


**Fig. 4.** Diagram summarizing the anatomy of the golden mussel (light and SEM images) in which (A) an adult golden mussel with the valves open can be seen. (B) a highlight of the region of the foot of the mollusk in its (C) ventral and (D) dorsal portions, and (E) the byssus gland orifice situated at the base of the foot and (F) a live young golden mussel with its foot exposed observed with optical magnifying glass.

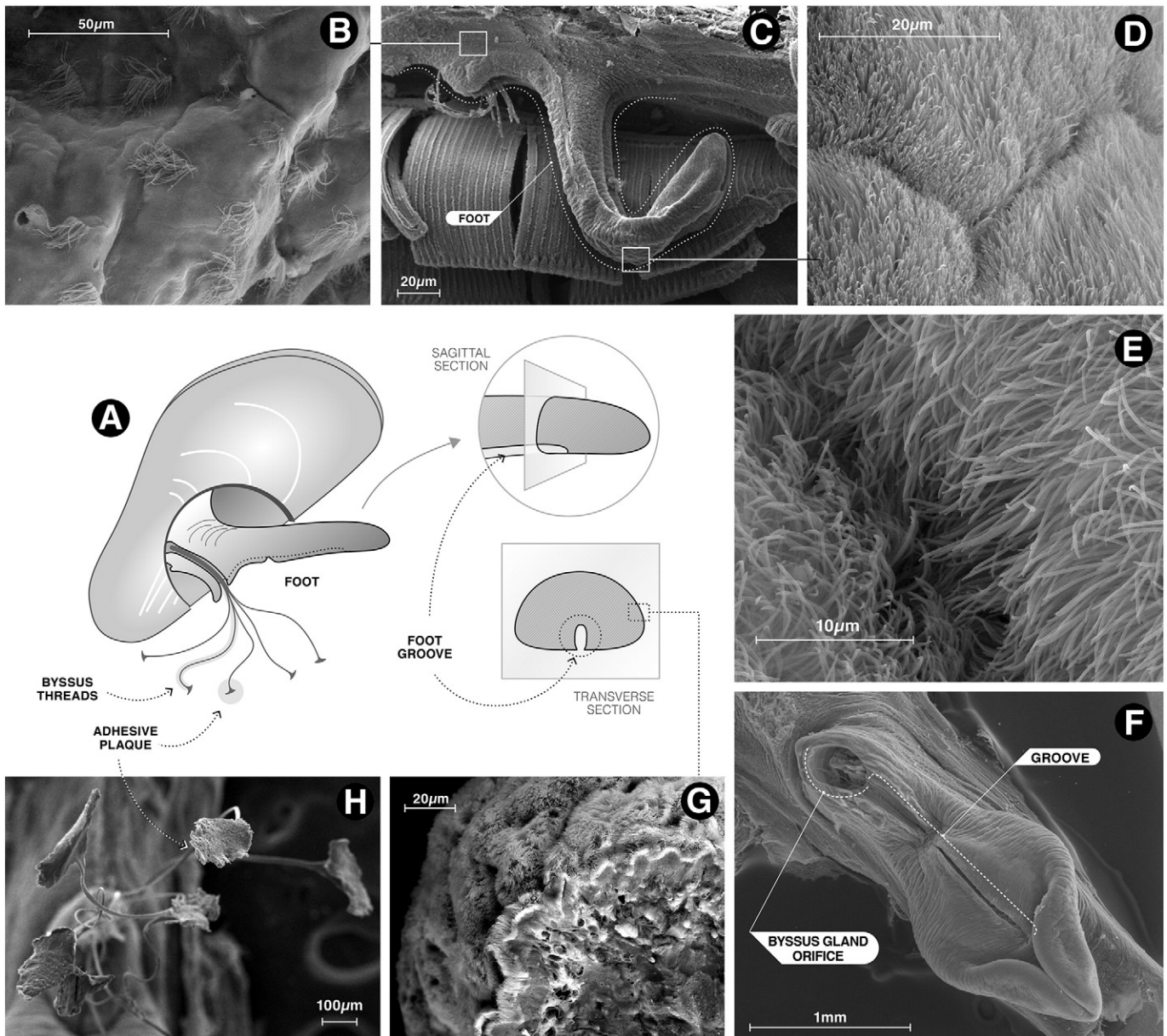


**Fig. 5.** (A) Illustration of a golden mussel highlighting the foot of the individual. (B) SEM of the region in which the foot merges with the visceral mass, presenting a low density of ciliary tufts (C) SEM image in which it is possible to observe the relaxed foot and some squashed byssus filaments coming out of the byssus gland orifice in the base of the foot. (D) Detail of the ventral portion of the foot covered by cilia. (E) Detail of the surface covered with cilia. (F) A panoramic image of the foot of *L. fortunei* highlighting the groove in the ventral region and a well defined byssus gland orifice. (G) SEM image of the foot fragment obtained from cryo-fracture. (H) SEM of byssus threads and adhesive plaques.

*Type C*: the cells in the tissue have an elliptical shape and exhibit a reduced amount of granules. The secretory granules are circular shaped with a mean diameter of  $0.92 \mu\text{m}$ . The electron density of these granules was the highest among the three, exhibiting a darker shade of gray and a concentric pattern (Fig. 8C).

### 3.2. Surface morphology and adhesion phenomenon

#### 3.2.1. Ciliary epithelium

The epithelial tissue could be characterized as ciliary epithelium due to the presence of axonemes (structures composed of nine pairs of microtubules in a circle, with a central pair), as can be seen in Fig. 9. The cilia found on the surface of the foot measured, on average,  $6.8 \mu\text{m}$  in length and  $0.2 \mu\text{m}$  in diameter each (Fig. 10).

The diameter of a foot measuring  $1445 \mu\text{m}$  (length) ranges from  $372 \mu\text{m}$  along the lateral plane to  $206 \mu\text{m}$  along the dorsoventral plane.

The estimated volume of the foot has been estimated in  $66 \times 10^6 \mu\text{m}^3$  and the surface area was  $13 \times 10^5 \mu\text{m}^2$ . The average density of cilia per square micrometer is 28.5.

#### 3.2.2. Estimating the strength of cilia–surface interaction

Table 1 shows the estimated values for cilia–surface interaction for various distances  $\ell$  between the cilium tip and any attachable surface. To calculate the energy of interaction between cilium and substrate equations of the free energy of interaction  $G$  [19,20] were employed. For the model sphere–plane interaction two situations were considered: one when the radius  $R$  of the cilium tip is much bigger than the distance cilium–surface ( $\ell \ll R$ )

$$G(\ell, R) = -\frac{A_H}{6} \frac{R}{\ell} \quad (1)$$

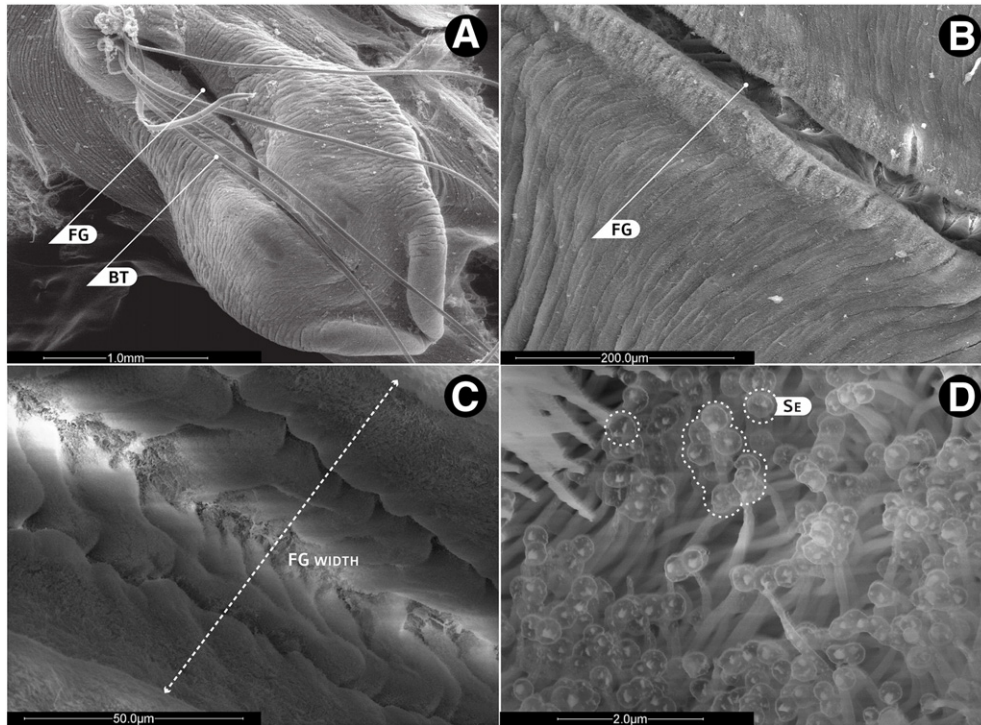


**Fig. 6.** SEM image showing the existence of a groove throughout the length of the foot. (A) Panoramic image showing the byssus threads (BT) and the foot groove (FC) which is involved in the molding of glandular secretions that will give form to the byssus. (B) Increased zoom on the ventral portion of the foot showing the edged of the groove (FC). (C) Detail of the interior of the groove (FC) covered with cilia. (D) Detail of the interior of the groove with secretions (Se) deposited on the surface of the cilia.

the van der Waals force per cilium is:

$$F(\ell, R) = -\frac{A_H}{6} R \ell^2. \quad (2)$$

The other situation is when there is a large separation ( $\ell \gg R$ )

$$G(\ell, R) = -\frac{2A_H}{9} \frac{R^3}{\ell^3} \quad (3)$$

the van der Waals force per cilium is

$$F(\ell, R) = -\frac{2A_H}{3} \frac{R^3}{\ell^4} \quad (4)$$

in which  $G$  is the free energy of interaction,  $A_H$  is the constant of Hamaker,  $R$  is the radius of the cilium tip (Fig. 6) and  $\ell$  is the distance between the cilium tip and the surface. The value of  $A_H$  was considered as  $9 \text{ zJ}$  for the interaction of proteins across water [19]. Values (from experiments or theory) for the Hamaker constant for two media interacting across another medium are few [20]. The protein–protein

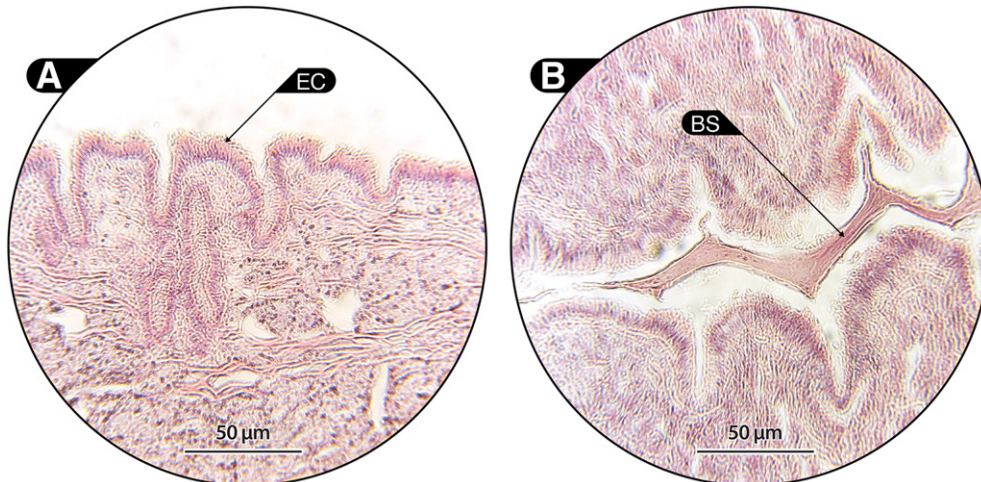


**Fig. 7.** Light microscopy of the *L. fortunei* foot, HE coloring. (A) Sagittal section showing the epithelial ciliary tissue (EC) on the surface of the foot. (B) Detail of the interior of the foot groove, delimited by epithelial ciliary tissue, where glandular byssal secretions (BS) could be found.

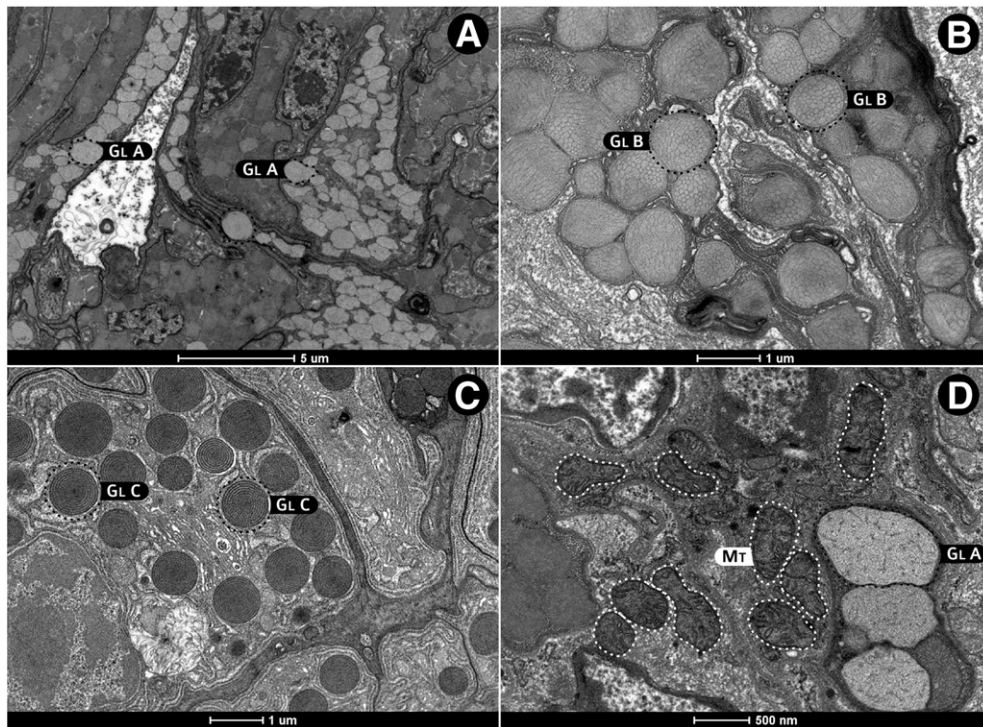


**Fig. 8.** Transmission electron microscopy (TEM) of the secreting cells on the foot of *L. fortunei*. (A) Secreting cells of the type A in the epithelial layer; the secretion beads (Gl A) present low electron density, exhibiting light shades of gray. (B) Secreting cells of the type B in the layer of connective tissue; the secretion beads (Gl B) present higher electron density than in A, but lower than in C, exhibiting medium shades of gray. Inside Gl B, it is possible to note the presence of tiny structures looking like other granules. (C) Secreting cells of the type C; the secretion beads (Gl C) presented high electron density, exhibiting darker shades of gray. Observe the concentric pattern inside each granule. (D) Detail of the presence of a large number of mitochondria (Mt) and secretion beads of the type A (Gl A), the most abundant in the whole tissue.

interaction across water was the closest situation to our case, bearing in mind the ubiquity of biofilms and their importance to the golden mussel attachment.

A third situation presented in Table 1 is based on the model of parallel extended surfaces assuming the foot of the mussel as a surface covered with dozens of millions of cilia. The average area of interaction was estimated to be about 40% of the total area of the foot calculated from SEM images resulting in  $540.000 \mu\text{m}^2$  for a young adult specimen. The equation that estimates the value of  $G$  necessary to bring two surfaces of an infinite separation to a finite separation  $\ell$  is

$$G(\ell, R) = -\frac{A_H}{12\pi\ell^2} \quad (5)$$

and the van der Waals force ( $F$ ) per cilium is

$$F(\ell, R) = -\frac{A_H}{6\pi\ell^3}. \quad (6)$$

Fig. 11 shows the points for the three situations calculated using the Eqs. (2), (4) and (6) and shown in Table 1. A dashed line indicates the average weight of an *L. fortunei* adult individual. The weighing procedure of twenty adult individuals of our aquarium of mussels is presented in Section 2.1. The adhesion strength (of around 15 million cilia) was calculated using Eq. (2). The result is close to the average weight of an adult mussel when cilium–surface distances are of the order of inter-atomic distances ( $>0.3 \text{ nm}$ ) and of the order of nanometers ( $\ell \leq 2.5 \text{ nm}$ ) when estimated from Eq. (6). If estimates are correct

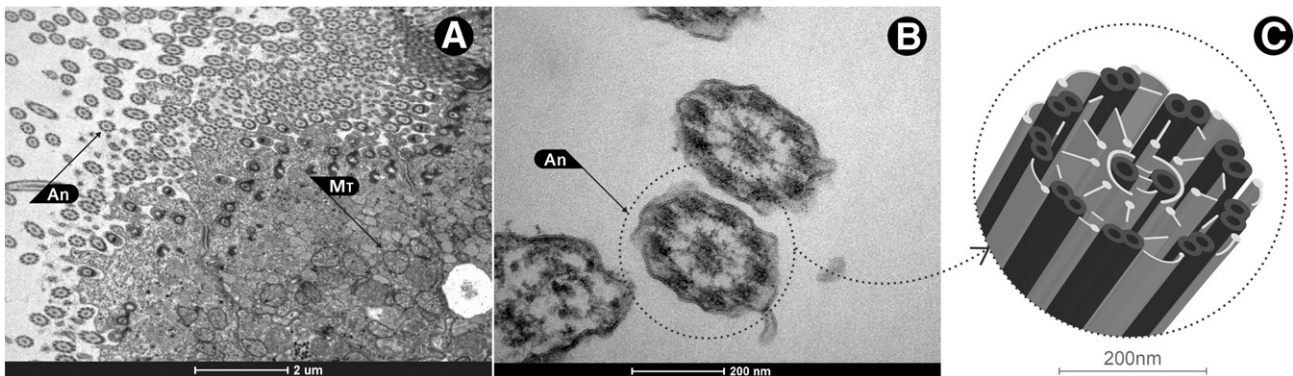


**Fig. 9.** Transmission electron microscopy image showing (A) a massive presence of axoneme (An) and mitochondria (Mt) along the epithelial tissue of the foot. (B) Detail of the composition of the axoneme, (An) formed by 9 pairs of microtubules around a central pair. (C) Three-dimensional representation of the Axoneme (An).

only when the cilia are close to a surface, the temporary adhesion force by van der Waals is sufficient to hold the mussel weight. Immersed in water the force between cilia and surfaces is altered from that in air or vacuum and the estimation above agrees with observation that the van der Waals attraction in water is reduced [27]. However, in water other forces can now arise that can qualitatively change the range of the interaction. This last case must be elucidated in order to develop more effective ways [38] to control the clogging of industrial water ducts by the *L. fortunei*.

#### 4. Discussion

The foot of *L. fortunei* is flattened and muscular, covered by cilia over its whole extension. A massive presence of axonemes (Fig. 5) found on the epithelium of the foot of *L. fortunei* confirms that the microstructures on the surface are true cilia. This finding was reinforced by the presence of mitochondria distributed along this tissue in the apical cytoplasm (Fig. 9D). Performing the technique of cryo-fracture (Fig. 1) it has been possible to obtain images of fragments that allowed us to visualize the foot *L. fortunei* in cross section and observe the communication between the structures and tissues of the interior and exterior of the foot and especially the ciliated epithelium. This technique allowed us to perform measurements of cilia and understand issues related to the functions that these structures are able to pursue.

The mean measures of cilium 6.8  $\mu\text{m}$  in length and 0.2  $\mu\text{m}$  in diameter (Fig. 6) were compatible to those found on the surface of red abalone foot (measuring approximately 0.2  $\mu\text{m}$  in diameter, which were inadequately named by the authors as nanofibrils). A peculiarity has been found in the form of the cilia of the foot of *L. fortunei* which has also drawn attention: the shape of each cilium found on the surface of the foot of *L. fortunei* is different from those already found in other mollusks [8,12,13,21]. The distal portion of each cilium is narrower (0.1  $\mu\text{m}$  in

**Table 1**

Estimative for the values of the free energy ( $G$ ) and the interaction force ( $F$ ) per cilium, and the interaction force ( $F$ ) between the cilia-covered foot area and a planar surface. Two models have been used: Model 1 is a sphere close to a planar thick wall in two situations: a) when tip radius is much bigger than the cilium-wall distance ( $R \gg \ell$ ); and situation b) when tip radius is much smaller than the cilium-wall distance ( $R \ll \ell$ ); Model 2 considers two surfaces separated by distance  $\ell$ , where mussel's foot is considered as a surface. Eqs. (2), (4) and (6) were employed to calculate free energy ( $G$ ) and the interaction force ( $F$ ) values. The constants used for the calculation are: Hamaker constant  $A_{H1} = 9 \times 10^{-21}$  J; gravity  $g = 9.80665$  m/s<sup>2</sup>; foot area  $\approx 540 \times 10^3$   $\mu\text{m}^2$ ; average mussel weight = 0.088 g; number of cilia per  $\mu\text{m}^2 = 28$ ; cilium tip radius  $\approx 50$  nm.

$\ell$ (nm)	$R/\ell$	Sphere near planar thick wall variable separation $\ell$			Infinity extended walls variable separation $\ell$			
		Free energy G per cilium (J)	Force per cilium (nN)	Total force (N)	Free energy G per cilium (J)	Total force (N)	Free energy G per cilium (J/m <sup>2</sup> )	Total force (N)
0.1	500	$7.5 \times 10^{-19}$	2.4	0.11			$2.4 \times 10^{-2}$	$2.6 \times 10^2$
0.5	100	$1.5 \times 10^{-19}$	$9.5 \times 10^{-2}$	$4.5 \times 10^{-3}$			$9.5 \times 10^{-4}$	2.0
1.0	50	$7.5 \times 10^{-20}$	$2.4 \times 10^{-2}$	$1.1 \times 10^{-3}$			$2.4 \times 10^{-4}$	$2.6 \times 10^1$
5	10	$1.5 \times 10^{-20}$	$9.5 \times 10^{-4}$	$4.5 \times 10^{-5}$			$9.5 \times 10^{-5}$	$2.0 \times 10^3$
10	5	$7.5 \times 10^{-21}$	$2.4 \times 10^{-4}$	$1.1 \times 10^{-5}$			$2.4 \times 10^{-5}$	$2.6 \times 10^4$
100	0.5				$2.5 \times 10^{-22}$	$3.8 \times 10^{-15}$	$2.4 \times 10^{-9}$	$2.6 \times 10^7$
500	0.1				$2.0 \times 10^{-24}$	$3.0 \times 10^{-17}$	$9.5 \times 10^{-10}$	$2.0 \times 10^9$
1000	0.05				$2.5 \times 10^{-25}$	$3.8 \times 10^{-18}$	$2.4 \times 10^{-10}$	$2.6 \times 10^{10}$
2000	0.025				$3.1 \times 10^{-26}$	$4.7 \times 10^{-19}$	$6.0 \times 10^{-11}$	$3.2 \times 10^{11}$

diameter) compared to the diameter of the rest of the stem (0.2  $\mu\text{m}$ ) and ends in a rounded tip (Fig. 6). This form and size can further facilitate adhesion by van der Waals forces as they come closer to the optimal measures pointed out in the literature by Gao and Yao and Arzt [22,23].

The van der Waals forces are highly dependent on the size and shape [19,22] and the proximity between both the body and the surface. The

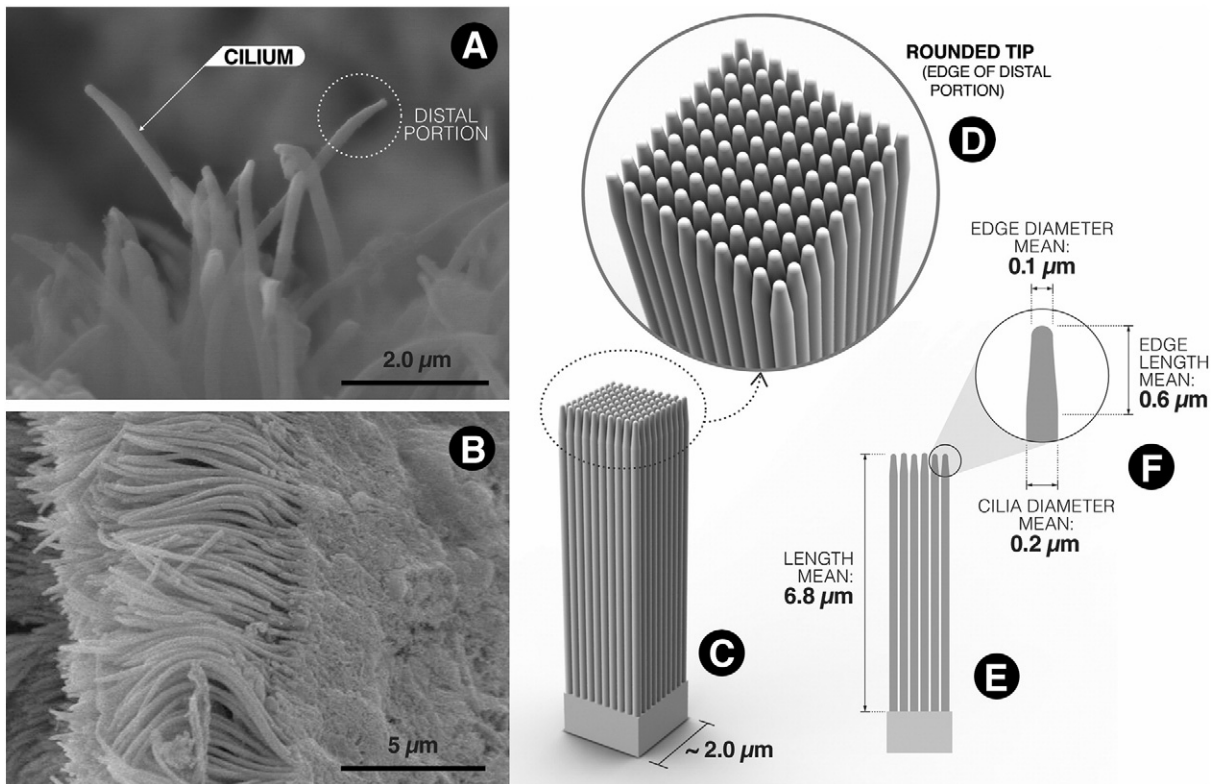


**Fig. 10.** Diagram showing (A) SEM image in which the peculiar shape of the cilia covering the surface of *L. fortunei* foot could be noticed. Each cilium has a narrowing on its distal portion with a rounded tip on the edge. (B) Cryofracture SEM image showing the density of the cilia on the surface of the foot. (C) 3D simulation of an average square on surface with an area of 10  $\mu\text{m}^2$ . (D) 3D simulation of the distal portion of the cilia showing the rounded tips of the edge. (E) Average dimensions of the cilia obtained utilizing the Software *ImageJ*. (F) Average dimensions of cilia tip obtained utilizing the Software *ImageJ*.

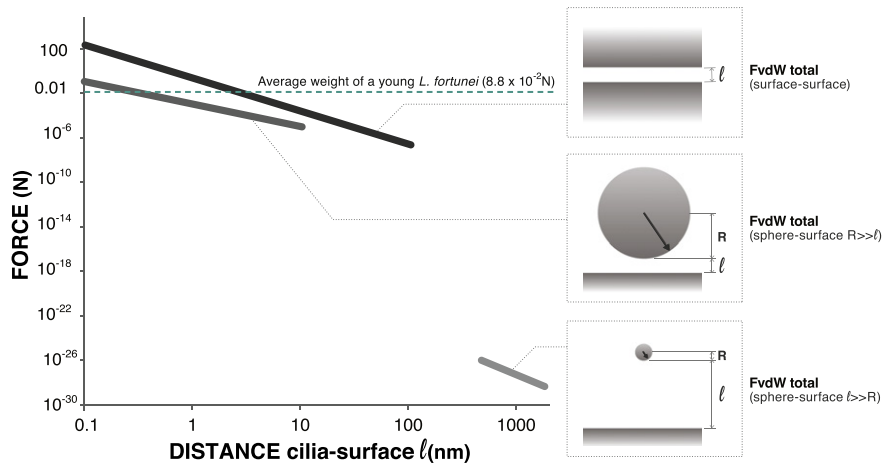


**Fig. 11.** Plot for the calculated values of the interaction force  $F$  between the cilia-covered foot area and a planar surface. Two models have been used: Model 1 is a sphere close to a planar thick wall in two situations: a) when tip radius is much bigger than the cilium-wall distance ( $R \gg \ell$ ); and situation, b) when tip radius is much smaller than the cilium-wall distance  $\ell$  ( $R \ll \ell$ ); Model 2 considers two surfaces separated by distance  $\ell$ , where mussel's foot is considered as a surface. The dashed line is the value of the average weight of a young adult *Limnoperna fortunei* mussel. Eqs. (2), (4) and (6) were used to calculate  $F$  values. The constant values used for the calculation are presented in Table 1. The constants used for the calculation are: Hamaker constant  $A_H = 9 \times 10^{-21}$  J; gravity  $g = 9.80665$  m/s<sup>2</sup>; foot area  $\approx 540 \times 10^3$   $\mu\text{m}^2$ ; average mussel weight = 0.088 g; number of cilia per  $\mu\text{m}^2 = 28$ ; cilium tip radius  $\approx 50$  nm.

presence of cilia covering the foot of mollusks can act as highly specialized structure for underwater adhesion through van der Waals forces and that ability was demonstrated in the study of the gastropod Red Abalone, *H. rufescens* [12].

High values of adhesion force can be found on the interaction between two surfaces with a fixed distance between them (Fig. 12A), as it can be seen in Table 1 and Fig. 11. The value of the adhesion strength is reduced when considering other shapes, such as the interaction between a sphere and a plane (Fig. 12B and C), which seemed to be the case of the ciliated surface of the foot (considering that each cilium has a semi-spherical tip).

The massive presence of cilia (Fig. 1), however, and the conforming properties of the whole structure of the foot can considerably increase

the bondability to the substrates and we can say that it behaves like a conforming surface (Fig. 12D and E) easily fitting even rough or non-flat surfaces of substrates. This phenomenon is similar to the one observed in adhesive toe pads of gekkonid lizards [3] where micro- and nano-hierarchical structures play a major role on increasing the area of contact. The size of each individual cilia also allows it to conform even to surfaces with nano-roughness of about 100 nm. The soft composition of the material forming the cilia also apparently allows deformations that make it fit in nano-scale to the format of substrates, as shown in Fig. 13. These small changes in which occurrence is estimated could further provide an increase of the van der Waals forces. Thus, we can estimate that the quantitative result would be between the lines a and b of Fig. 11. These results would be consistent with observations in the

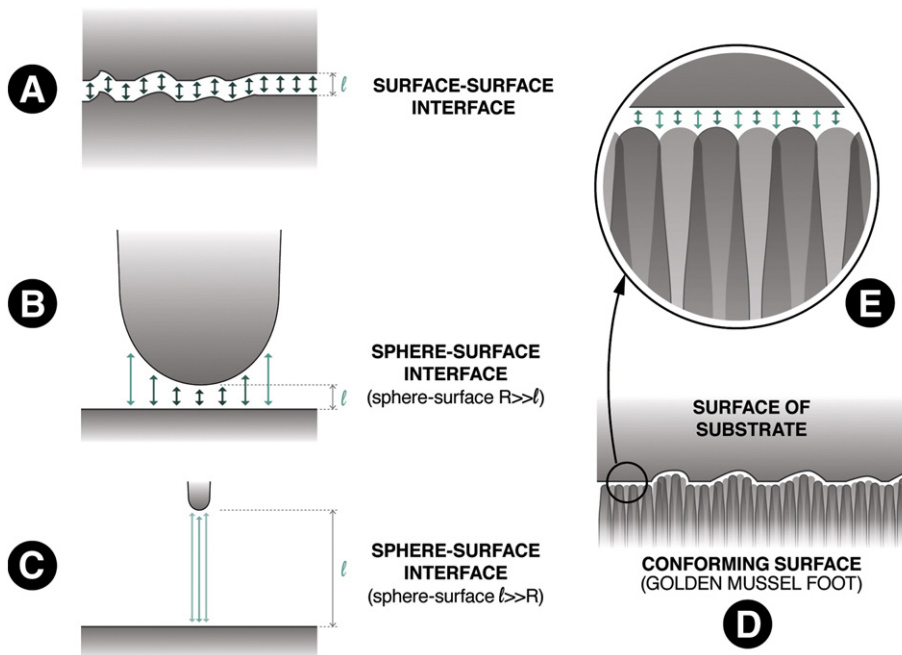


**Fig. 12.** (A) Illustration of the interaction between two surfaces through Van der Waals forces. (B) Illustration of the interaction between a plane and a semi-sphere in which the distance  $\ell$  is much smaller than the radius. (C) Illustration of the interaction between a plane and a semi-sphere in which the distance  $\ell$  is much larger than the radius. (D) Diagram illustrating the interaction between the ciliated surface of the foot of the golden mussel and a hypothetical surface. The ciliated surface conforms to substrate thus increasing the contact area and therefore the forces of Van der Waals interaction. (E) Detail in the previous diagram highlighting the increased contact area due to the conformation of ciliary surface.

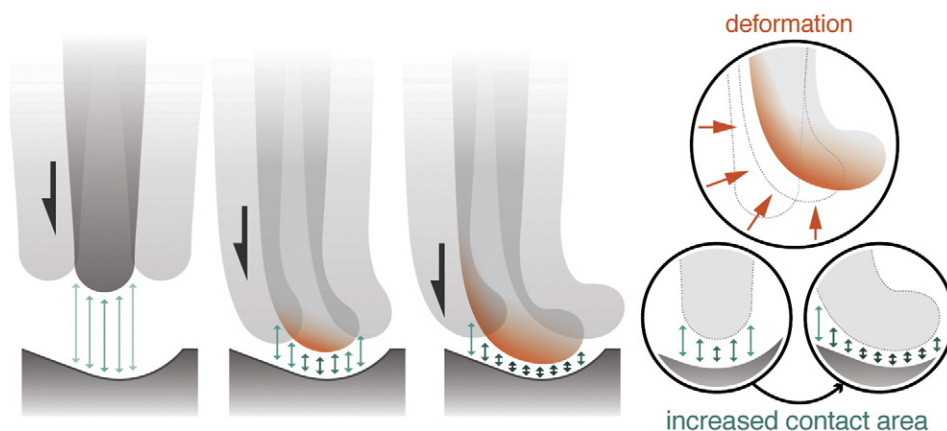


**Fig. 13.** Diagram representing an envisaged situation where a cilium could undergo deformation in nano-scale due to the contact to the surfaces which could result in an increase of van der Waals forces.

laboratory of the animal moving around easily on both glass surface of aquaria, waxy hydrophobic surfaces of plants and even on the water surface.

The presence of ciliary structures is also reported in the literature as a facilitator of transportation of aquatic animals (such as in *Daphnia* sp.) in view of the increased viscosity of the fluid due to the scale of these aquatic species [24]. This property is certainly a great help for the larval stage of the golden mussel, which is the main way of its spreading as invasive species.

Also, these structures can contribute to facilitate movement of substances and particles entering the mantle cavity as well as to carry mucous substances out of the cavity of the mantle [8,25,26]. This also explains the advantages of the presence of ciliated surface inside the groove of the foot (Figs. 3 and 8), which is delimited by a ciliary epithelial tissue and frequently presents mucous secretions within its whole of its extension (Figs. 3 and 9). A similar structure was found in other species also pertaining to the family Mytilidae, the *M. edulis* [13,28] which was related to the locomotion and attachment of the animal to the substrate transporting the secretions to the base of the foot to form the byssus threads [29–31]. Both in attaching as in burrowing bivalves, there is the presence of secreting glands, which perform functions adapted to the habitat of each group. In the case of burrowing bivalves, they are used primarily for the fixing of sediments and formation of pseudofeces [32,33]. In the attaching bivalves (mussels) on the other hand they seem to be associated with the formation of the permanent fixing device [34, 35], known as byssus [18,28,36,37].

In our experiments glandular secretions were found over the extension of the foot groove (Fig. 3), which confirms the function of the channel in the migration of the adhesive secretions for the formation of the byssus threads and the adhesive plate. As found in the literature and also confirmed by the performed experiments, the secretory apparatus found is not linked to the temporary adhesion to substrates, which seems to be performed mostly by the van der Waals forces provided by the interaction between the ciliated surface and the substrate since we could estimate adequate values for it.

The functional surface of foot of the golden mussel, *L. fortunei*, is involved in locomotory processes in the aquatic medium, temporary adhesion for locomotion and in the production, secretion, and migration of substances for the formation of byssus which could confirm the significant importance of this structure to the exploration and selection and of a settlement site.

### Acknowledgments

The authors would like to acknowledge the Companhia Energética de Minas Gerais (Cemig GT) for providing financial support to this research. We would also like to thank professors Hélio Chiarini-Garcia

and Elizete Rizzo Bazzoli, from Institute of Biological Sciences (ICB) of Federal University of Minas Gerais (UFMG) and the Centre of Microscopy of the same university ([www.microscopia.ufmg.br](http://www.microscopia.ufmg.br)) for providing the equipment and technical support for experiments involving optical and electron microscopy.

### References

- [1] S.N. Gorb (Ed.), *Functional Surfaces in Biology: Adhesion Related Phenomena*, vol. 2, Springer, 2009.
- [2] G. Huber, S.N. Gorb, R. Spolenak, E. Arzt, Resolving the nanoscale adhesion of individual gecko spatulae by atomic force microscopy, *Biol. Lett.* 1 (2005) 2–4.
- [3] K. Autumn, A.M. Peattie, Mechanisms of adhesion in geckos, *Integr. Comp. Biol.* 42 (2002) 1018–1090.
- [4] W.J. Barnes, Functional morphology and design constraints of smooth adhesive pads, *MRS Bull.* 32 (2007) 479–485.
- [5] E.M. Gosling, *Bivalve Molluscs: Biology, Ecology, and Culture*, Fishing News Books, Oxford; Malden, MA, 2003.
- [6] S.L. Brazeel, Carrington, Interspecific comparison of the mechanical properties of mussel byssus, *Biol. Bull.* 11 (3) (2006) 263–274.
- [7] N. Holten-Andersen, N. Slack, F. Zok, J.H. Waite, Nano-mechanical investigation of the byssal cuticle, a protective coating of a bio-elastomer, *Mater. Res. Soc. Symp. Proc.* 844 (2005).
- [8] J.S. Lee, Y.G. Lee, J.J. Park, Y.K. Shin, Microanatomy and ultrastructure of the foot of the infaunal bivalve *Tegillarca granosa* (Bivalvia: Arcidae), *Tissue Cell* 44 (2012) 316–324.
- [9] Q. Lu, D.S. Hwang, Y. Liu, H. Zeng, Molecular interactions of mussel protective coating protein, mcp-1, from *Mytilus californianus*, *Biomaterials* 33 (2012) 1903–1911.
- [10] F.D. Passos, O. Domanechi, A.F. Sartori, Biology and functional morphology of the pallial organs of the Antarctic bivalve *Mysella charcoti* (Lamy, 1906) (Galeommatoidae: Lasaeidae), *Polar Biol.* 28 (2004) 372–380.
- [11] A.G. Punt, G.E. Millward, M.B. Jones, Uptake and depuration of 63 Ni by *Mytilus edulis*, *Sci. Total Environ.* 214 (1998) 71–78.
- [12] A.Y.M. Lin, R. Brunner, P.Y. Chen, F.E. Talke, M.A. Meyers, Underwater adhesion of abalone: the role of van der Waals and capillary forces, *Acta Mater.* 57 (2009) 4178–4185.
- [13] C.H. Brown, Some structural proteins of *Mytilus edulis*, *Q. J. Microsc. Sci.* 3 (1952) 487–502.
- [14] Z. Jiang, L. Du, X. Ding, H. Xu, Y. Yu, Y. Sun, Q. Zhang, *Mater. Sci. Eng. C* 32 (2012) 1280–1287.
- [15] R. Seed, C.A. Richardson, Evolutionary traits in *Perna viridis* (Linnaeus) and *Septifer virgatus* (Wiegmann) (Bivalvia: Mytilidae), *J. Exp. Mar. Biol. Ecol.* (1999) 273–287.
- [16] E. Brugnoli, J. Clemente, L. Boccardi, A. Borthagaray, F. Scarabino, Golden mussel *Limnoperna fortunei* (Bivalvia: Mytilidae) distribution in the main hydrographical basins of Uruguay: update and predictions, *An. Acad. Bras. Cienc.* 77 (2005) 235–244.
- [17] W. Collyer, C. Jurídica, Ballast water, bioinvasion and international reply (Portuguese), *Rev. Jurídica* 9 (2007) 145–160.
- [18] A. Tamarin, P.J. Keller, An ultrastructural study of the byssal thread forming system in *Mytilus*, *J. Ultrastruct. Res.* 40 (1972) 401–416.
- [19] V.A. Parsegian, *Van der Waals Forces: A Handbook for Biologists, Chemists, Engineers, and Physicists*, Cambridge Univ Press, 2005.
- [20] J.N. Israelachvili, *Intermolecular and Surface Forces*, Acad. Press, 2011.
- [21] J.J. Park, J.S. Lee, Y.G. Lee, J.W. Kim, Micromorphology and Ultrastructure of the Foot of the Equilateral Venus *Gomphina veneriformis* (Bivalvia: Veneridae), *Open Journal of Cell Biology*, 2012.
- [22] H.H. Gao, H.H. Yao, Shape insensitive optimal adhesion of nanoscale fibrillar structures, *Proc. Natl. Acad. Sci. U. S. A.* 101 (2004) 7851–7856.

- [23] E. Arzt, Biological and artificial attachment devices: lessons for materials scientists from flies and geckos, *Mater. Sci. Eng. C* 26 (2006) 1245–1250.
- [24] S. Vogel, *Comparative Biomechanics: Life's Physical World*, Princeton University Press, 2003.
- [25] P.G. Beninger, S. St-Jean, Y. Poussart, J.E. Ward, Gill function and mucocyte distribution in *Placopecten magellanicus* and *Mytilus edulis* (Mollusca: Bivalvia): the role of mucus in particle transport, *Mar. Ecol. Prog. Ser.* 98 (1993) 275–282.
- [26] P. Beninger, A. Veniot, The oyster proves the rule: mechanisms of pseudofeces transport and rejection on the mantle of *Crassostrea virginica* and *C. gigas*, *Mar. Ecol. Prog. Ser.* 190 (1999) 179–188.
- [27] B. Bhushan, *Nanotribology and Nanomechanics II*, Springer Science & Business Media, 2011.
- [28] K.J.K. Coyne, J.H.J. Waite, In search of molecular dovetails in mussel byssus: from the threads to the stem, *J. Exp. Biol.* 203 (2000) 1425–1431.
- [29] I.M. Côté, Effects of predatory crab effluent on byssus production in mussels, *J. Exp. Mar. Biol. Ecol.* 188 (1995) 233–241.
- [30] A.F. Eble, Anatomy and histology of *Mercenaria mercenaria*, in: J.N. Kraeuter, M. Castagna (Eds.), *Biology of the Hard Clam*, Elsevier, New York 2001, pp. 117–220.
- [31] J.H. Waite, X.-X. Qin, K.J. Coyne, The peculiar collagens of mussel byssus, *Matrix Biol.* 17 (1998) 93–106.
- [32] H.J. Cranfield, Observations on the function of the glands of the foot of the pediveliger of *Ostrea edulis* during settlement, *Mar. Biol.* 22 (1974) 211–223.
- [33] J.L. Norenburg, J.D. Ferraris, Cytomorphology of the pedal aperture glands of *Mya arenaria* L. (Mollusca, Bivalvia), *Can. J. Zool.* 68 (1990) 1137–1144.
- [34] N.I. Selin, E.E. Vekhova, Morphological adaptations of the mussel *Crenomitilus grayanus* (Bivalvia) to attached life, *Russ. J. Mar. Biol./Biol. Morya* 29 (2003) 230–235.
- [35] L.V. Zuccarello, Ultrastructural and cytochemical study on the enzyme gland of the foot of a mollusc, *Tissue Cell* 13 (1981) 701–713.
- [36] A. Sobieszek, The fine structure of the contractile apparatus of the anterior byssus retractor muscle of *Mytilus edulis*, *J. Ultrastruct. Res.* 43 (1973) 313–413.
- [37] X.X. Qin, J.H. Waite, A potential mediator of collagenous block copolymer gradients in mussel byssal threads, *Proc. Natl. Acad. Sci. U. S. A.* 95 (1998) 10517–10522.
- [38] M. Xu, et al., Experimental study on control of *Limnoperna fortunei* biofouling in water transfer tunnels, *J. Hydro Environ. Res.* (2014) 1–11.